Polymers **2015**, *7*, 1020-1045; doi:10.3390/polym7061020

OPEN ACCESS

polymers

ISSN 2073-4360

www.mdpi.com/journal/polymers

Article

Interlaminar Fracture Toughness of CFRP Laminates Incorporating Multi-Walled Carbon Nanotubes

Elisa Borowski [1], Eslam Soliman [2], Usama F. Kandil [3] and Mahmoud Reda Taha [1,*]

[1] Department of Civil Engineering, University of New Mexico, MSC01 1070, Albuquerque, NM 87131, USA; E-Mail: eborowsk@unm.edu

[2] Department of Civil Engineering, Assiut University, Assiut 71516, Egypt; E-Mail: eslam.soliman@eng.au.edu.eg

[3] Polymer Nanocomposites Center, Egyptian Petroleum Research Institute, 1 Ahmed El-Zomor Street, Nasr City, Cairo 11727, Egypt; E-Mail: alfa_olefins@yahoo.com

* Author to whom correspondence should be addressed; E-Mail: mrtaha@unm.edu; Tel.: +1-505-277-1258; Fax: +1-505-277-1988.

Academic Editors: Alper Ilki, Masoud Motavalli

Received: 28 March 2015 / Accepted: 29 May 2015 / Published: 5 June 2015

Abstract: Carbon fiber reinforced polymer (CFRP) laminates exhibit limited fracture toughness due to characteristic interlaminar fiber-matrix cracking and delamination. In this article, we demonstrate that the fracture toughness of CFRP laminates can be improved by the addition of multi-walled carbon nanotubes (MWCNTs). Experimental investigations and numerical modeling were performed to determine the effects of using MWCNTs in CFRP laminates. The CFRP specimens were produced using an epoxy nanocomposite matrix reinforced with carboxyl functionalized multi-walled carbon nanotubes (COOH–MWCNTs). Four MWCNTs contents of 0.0%, 0.5%, 1.0%, and 1.5% per weight of the epoxy resin/hardener mixture were examined. Double cantilever beam (DCB) tests were performed to determine the mode I interlaminar fracture toughness of the unidirectional CFRP composites. This composite material property was quantified using the critical energy release rate, G_{IC}. The experimental results show a 25%, 20%, and 17% increase in the maximum interlaminar fracture toughness of the CFRP composites with the addition of 0.5, 1.0, and 1.5 wt% MWCNTs, respectively. Microstructural investigations using Fourier transform infrared (FTIR) spectroscopy and X-ray photoelectron spectroscopy (XPS) verify that chemical reactions took place between the COOH–MWCNTs and the epoxy resin, supporting the improvements experimentally observed in the interlaminar fracture toughness

of the CFRP specimens containing MWCNTs. Finite element (FE) simulations show good agreement with the experimental results and confirm the significant effect of MWCNTs on the interlaminar fracture toughness of CFRP.

Keywords: carbon nanotubes; fracture toughness; FTIR; XPS; finite element modeling

1. Introduction

Like most high-performance composites, carbon fiber reinforced polymers (CFRP) feature favorable material properties of a high strength-to-weight ratio and notable stiffness, making them ideal candidates for use in a broad range of industries, including aerospace, marine, armor, automotive, electronic, and infrastructural applications [1,2]. Additionally, CFRPs exhibit impressive in-plane tensile strength, resistance to tension-tension fatigue, impact resistance, durability [3], and corrosion resistance [4]. However, while CFRP composites have many optimal qualities, they also present several drawbacks, including poor in-plane compression, tension-compression fatigue, and restricted resistance to interlaminar fiber-matrix cracking and delamination due to the limited fracture toughness of the polymer matrices [5].

Interlaminar delamination is a major challenge in the design of composite structures. Within the matrix-dominated interlaminar region, brittle failure has been reported to manifest in the form of matrix transverse cracking and/or fiber-matrix interface debonding, both of which can severely affect the structural integrity of the composite laminate [3]. Delamination between composite layers is often initiated by imperfections introduced during the layup fabrication process. Micro-crack propagation then follows in regions of relatively high void content under conditions of transverse loading, impact stresses, fatigue, or various environmental factors [3,6]. Many studies have successfully quantified the relatively low fracture toughness of laminated composites. For example, Tamuzs *et al.* reported that the critical energy release rate of laminate composites does not commonly exceed 0.2–0.4 kJ/m^2 [6]. For the past several decades, the improvement of interlaminar fracture toughness in composites with brittle matrices has been a critical area of research and investigation.

Lubineau *et al.* [7] have distinguished between low/micro-scale and ply/meso-scale mechanisms of degradation. At the low/micro-scale, mechanisms of degradation consist of diffused intralaminar damage, diffused interlaminar damage, and fiber breakage. Diffused intralaminar damage occurs as shear-induced damage homogenously distributed throughout the thickness of the ply such as fiber/matrix debonding or small matrix cracks resulting in a decrease in stiffness with no visible transverse cracking. Diffused interlaminar damage is a shear-induced damage caused by micro-voids in the interlaminar interface matrix resulting in reduced stiffness without visible delamination. Fiber breakage is a statistical distribution of flaws in the material. At the ply/meso-scale, transverse cracking is observed as a crack that propagates completely across the thickness of a ply, and local delamination happens at the ply-to-ply interface resulting from overloading at the transverse crack tip.

There have been a number of attempts to improve out-of-plane properties through mechanical and materials solutions. Transverse stitching [8,9] and pinning [10,11] were two such examples of mechanical approaches. Micro-phase particles have also been examined, including rubbery or thermoplastic polymers [12] and the use of a midplane interleaf thickened with micro-particles [13,14].

Carbon nanotubes (CNTs) have been utilized as nanofillers for the enhancement of mechanical properties of polymers [15,16]. CNTs have remarkable strength and stiffness properties, and as such, are optimal constituents for use in composite laminates [5,7]. CNTs display a high aspect ratio, highly flexible elastic behavior during loading [2], low density, and a unique atomic structure, contributing to an improvement in load transfer and the ability to enhance the mechanical properties of CFRPs [17,18]. Within a brittle matrix such as epoxy, CNTs are able to function as a toughening material by bridging the lamina interfaces. Studies report that in addition to increasing the tensile strength, tensile modulus [2,15,17], flexural strength, and flexural modulus of epoxy [19], incorporating CNTs into a polymer matrix can limit creep and enhance the shear strength of the matrix [20], as well as improve the fracture toughness of the composite [18,21].

Aside from the benefits that CNTss provide, their application in composites presents two major challenges: a homogeneous dispersion of CNTs inside the polymer matrix and the occurrence of a chemical interaction between the CNTs and polymers. The high surface area of CNTs generates strong intrinsic van der Waals forces between individual tubes, causing CNTs to agglomerate and hold together in bundles [2,3]. As the CNTs content increases, this phenomenon becomes more pronounced [2]. Beyond a certain content of CNTs, they aggregate easily and function as a defect in the composite, contributing to stress concentrations and weakening the composite. Therefore, during composite fabrication it is necessary to avoid agglomerations as well as to maintain stable dispersion to avoid secondary agglomeration during curing [22]. Agglomerations cause CNTs to have a very low solubility in most solvents, often resulting in a non-homogenous dispersion within a surrounding matrix. Homogenous dispersion is crucial for matrix enhancement, because it increases the surface area of nanotubes that is available for interaction with the matrix [23]. The disentanglement of CNTs agglomerations also improves the quality of resin flow. Furthermore, it is likely that bundling can cause defects in the CNTs. For these reasons when CNTs are highly entangled, the mechanical properties of the composite become impaired [24]. Therefore, it is essential to ensure the homogeneous dispersion of CNTs throughout a composite matrix.

Several techniques have been shown to improve compatibility between CNTs and matrices, including mechanical stirring, sonication, centrifugal mixing, oxidation/filtration protocol, chemical modification of CNT surface, and the use of surfactants such as dispersants and block copolymers [25]. CNTs can be dispersed in an epoxy matrix using high-shear mixing or attached directly to the fiber surface using a sizing coating [26]. Lubineau *et al.* [7] discuss a variety of additional ways CNTs can be applied to a composite. They can be introduced in the gaseous phase using chemical vapor decomposition to grow CNTs directly on the fiber surface. They can be introduced in the liquid phase using electrophoresis to deposit CNTs on the dry fabric surface or using mechanical coating to cover the dry fiber with a sizing agent. Alternatively, the CNTs can be introduced directly into the matrix using several techniques including solvent casting (ultra-sonication, mechanical stirring, or magnetic stirring), melt mixing, and *in situ* polymerization. Classical manufacturing processes include hand-layup, resin transfer molding, vacuum impregnation, and the use of pre-impregnated materials. Random dispersion can be achieved through a variety of means including powder dispersion, spraying, roll coating, and electro-spinning. The techniques used in this paper foreseen to reduce agglomeration are functionalization, ultra-sonication, and high speed mechanical mixing.

A strong chemical bond between CNTs and polymers is necessary for load transfer to occur between the epoxy matrix and the nanotubes. If the interfacial chemical interactions between the CNTs and the matrix are weak, the CNTs can be pulled out during delamination, limiting the enhancement of fracture toughness that they are able to provide [27]. Several studies have utilized the functionalization of CNTs to improve dispersion and chemical bond [3,5,24]. Functionalized groups produce strong covalent bonds between the CNTs and the epoxy matrix, forming a highly cross-linked composite structure [23]. This cross-linking allows the load to be effectively transferred from the matrix to the CNTs, resulting in improved strength and fracture toughness of the composite. Moreover, it has been shown that functionalized CNTs exhibit better dispersion inside an epoxy matrix than non-functionalized CNTs [2]. This improved dispersion is due to the electrical charges of the functional groups counteracting the van der Waals forces of the CNTs [20], thus increasing the available surface area of the nanotubes and improving the interaction between the CNTs and the epoxy matrix. For instance, Mujika *et al.* investigated the effect on interlaminar fracture toughness of twelve-ply unidirectional CFRP composites incorporating carboxylic and alcohol functionalized MWCNTs and non-functionalized MWCNTs. While the non-functionalized MWCNTs did not have an effect on the fracture toughness, the addition of 0.1 wt% functionalized MWCNTs showed a 22% increase in initiation fracture toughness and a 14% increase in propagation fracture toughness [28]. Previous research by the authors showed that the 1.0 wt% functionalized carboxyl multi-walled carbon nanotubes (COOH–MWCNTs) out-performed similar content of pristine MWCNTs in regard to the four-point flexural strength of epoxy nanocomposites and the in-plane shear strength of woven fabric composite coupons by 43% and 20%, respectively [20].

In this study, experimental and numerical investigations were conducted to examine the effect of incorporating COOH–MWCNTs in the epoxy matrix of unidirectional CFRP laminates tested for mode I interlaminar fracture toughness using DCB specimens. Our hypothesis is that the incorporation of MWCNTs will provide additional resistance against interlaminar cracking and delamination, therefore improving the fracture toughness of CFRP composite laminates.

2. Experimental Methods

2.1. Materials

The DCB composite laminate coupons were fabricated using a unidirectional carbon fiber fabric made of PANEX@35 carbon fibers formed from high capacity polyacrylonitrile (PAN) processing methods by Zoltek, St. Louis, MO, USA. The manufacturers report a tensile strength of 3860 MPa and a tensile modulus of elasticity of 242 GPa. The epoxy mixture consisted of a 635 thin epoxy resin mixed with a 2:1 ratio slow epoxy hardener by US Composites, West Palm Beach, FL, USA. It had a curing time of 24–28 h and a viscosity of 600 cps. The nanoscale constituents used were COOH–MWCNTs supplied by Cheap Tubes, Inc., Cambridgeport, VT, USA. They had an outer diameter of 20–30 nm, an inner diameter of 5–10 nm, and a length of 10–30 μm with purity greater than 95% by weight. The COOH functionalized groups were 1.23% by weight of the MWCNTs. While several types of functionalized MWCNTs groups, including ozone [24], amino [3], and fluorine [5], have been investigated for the purposes of improved dispersion and increased bonding, this research focuses on the incorporation of COOH–MWCNTs. One of the benefits of using COOH–MWCNTs is that both the surface and the ends of each nanotube carry more than one carboxylic acid group, which provides additional cross-linking [23].

Li *et al.* [15] reported that compared to hydroxyl functionalized carbon nanotubes (OH–CNTs), carboxyl functionalized carbon nanotubes (COOH–CNTs) are more stable in deionized water due to the presence of more surface functional groups. COOH–CNTs also provide more uniform and thicker coatings on carbon fiber fabric due to their dimensions and dispersion. Their stability in water suspension makes them superior to pristine MWCNTs by allowing them to achieve good dispersion through ultra-sonication. Their greater quantity of surface functional groups increases the opportunities for reaction with the epoxy matrix, which improves interfacial bonding. In addition to van der Waals binding and chemical bonding, CNTs also provide mechanical interlocking between the matrix and the fibers, increased interfacial friction, and local strengthening of the matrix at the interface. Cui *et al.* [22] showed that COOH–MWCNTs improved homogeneous dispersion and the interfacial adhesion between nanoparticles and epoxy. Figure 1 displays the chemical structure of epoxy and its potential interaction with COOH–MWCNTs.

Davis *et al.* investigated mode II interlaminar shear fracture toughness of 20-ply CFRP laminates incorporating fluorine-functionalized carbon nanotubes (F–CNTs). They found a 27% increase in average crack propagation, G_{IIC}, in specimens containing 0.5 wt% F–CNTs [5]. Romhany *et al.* studied the effect of adding 0.3 wt% non-functionalized MWCNTs to 10-ply unidirectional CFRPs using a three roll milling technique and found a 13% increase in the average fracture toughness compared to neat specimens [29]. Almuhammadi *et al*. fabricated 16-ply unidirectional CFRP laminates using a MWCNTs-liquid solution sprayed onto carbon fiber composite prepreg plies. They found a 17% increase in mode I fracture toughness by incorporating 0.5 wt% COOH–MWCNTs [30]. To our knowledge, the use of COOH–MWCNTs has never before been studied for improving mode I fracture toughness of unidirectional CFRP composites fabricated using a hand-layup technique.

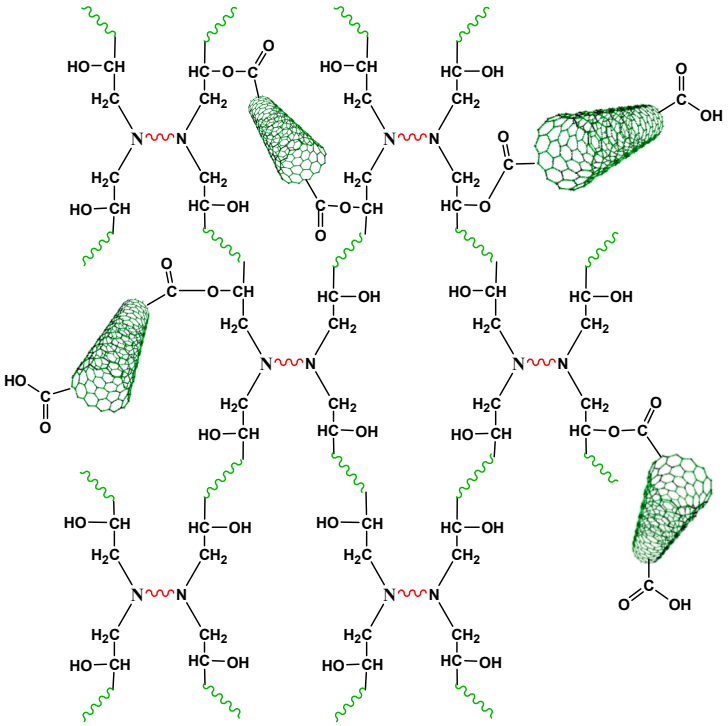

Figure 1. *Cont.*

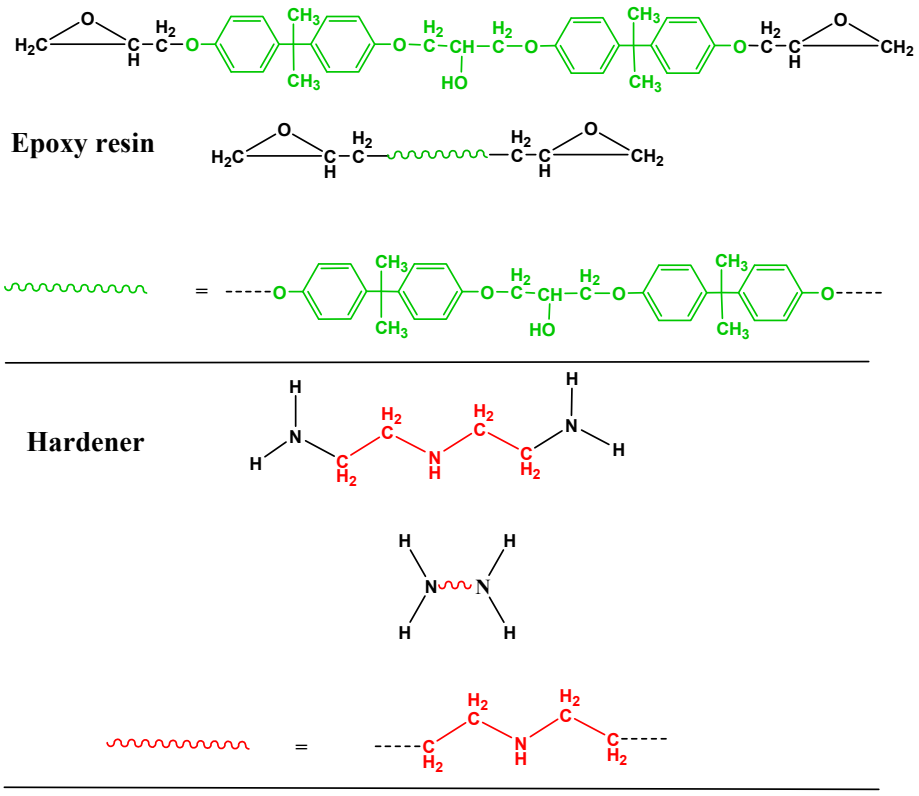

Figure 1. A schematic showing the chemical structure of epoxy and COOH–MWCNTs.

2.2. Dispersion of COOH–MWCNTs in Epoxy

The first step in preparing the CFRP nanocomposite laminates was to reinforce the epoxy resin with COOH–MWCNTs, following the method depicted in Figure 2. Four contents of MWCNTs were used in this study: 0.0% (neat epoxy), 0.5%, 1.0%, and 1.5% by weight of the neat epoxy resin/hardener mixture. To begin, the specified MWCNTs quantity was hand-stirred into the epoxy resin. The mixture was then degassed for five minutes and sonicated in an Ultrasonic System by Misonix, Farmingdale, NY, USA, for one hour at a temperature of 40 °C and a frequency of 40 kHz. The sonication process was performed to ensure the disentanglement of MWCNTs and consequently facilitating the chemical reaction between the resin and the COOH group. After sonication, the mixture was magnetically stirred for 2.0 h at a temperature of 80 °C and a speed of 700 rpm using a hotplate stirrer to decrease epoxy viscosity for a uniform dispersion of nanotubes. Both sonication and high speed magnetic stirring were used to break up nanotube agglomerates, create homogenous dispersion throughout the nanotube/epoxy mixture, and ensure the occurrence of chemical interactions between the functionalized groups of the MWCNTs and the resin. After stirring, the resin mixture was left to cool for approximately 1.0 h to reach room temperature. After cooling, the epoxy hardener was hand-stirred into the MWCNTs/resin mixture for 15 min, resulting in an epoxy-MWCNTs composite. The above dispersion method was based on a technique reported by Zhu *et al.* with positive results [23] and was verified in succeeding studies reporting homogeneous dispersion of MWCNTs [31].

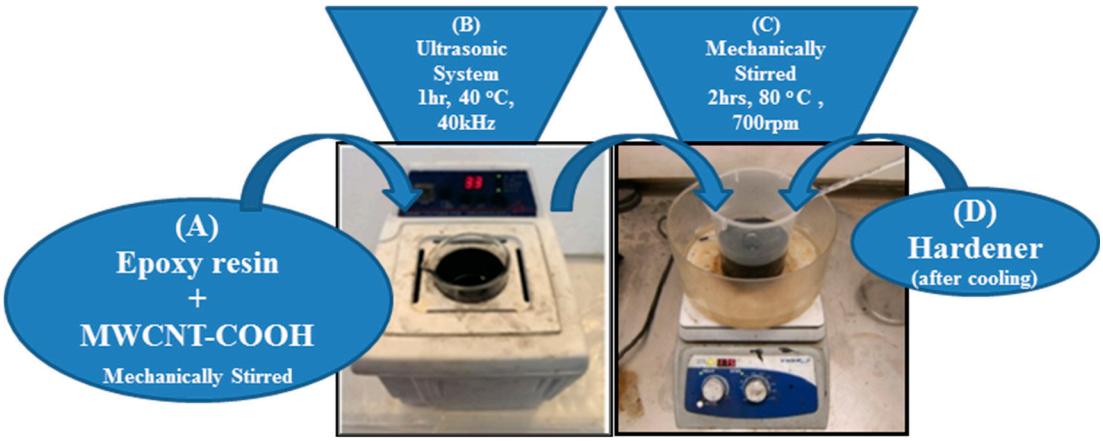

Figure 2. An outlined process for the dispersal of COOH–MWCNTs in epoxy.

2.3. Laminate Fabrication

The DCB specimens were fabricated in accordance with ASTM D5687 [32]. Numerous thin sheets were hand-layered atop a 457.2 mm^2 aluminum plate. As shown in Figure 3, the sheets consisted of the following: a non-porous release film, polyester peel ply, twelve layers of unidirectional carbon fiber fabric, a 0.0152 mm thick release film insert, a perforated release film, and a breather cloth. The carbon fiber fabric layers were stacked in the 0° direction. The release film was inserted along the midplane of the laminate to create an initial crack length of 50 mm from the point of loading to the crack tip. Laminate fabrication was completed using vacuum infusion. An airtight nylon bag was placed over the layup, and a vacuum hose was attached to generate a constant vacuum pressure of 3.07 Pa for the next 24 h. Once the vacuum hose was removed, each plate was left to cure at room temperature for six weeks before testing. Once dry, the laminate plates were cut along the fiber direction into 152.4 mm by 25.4 mm specimens. The exact width and thickness of each specimen were recorded and later used for fracture toughness analysis. It has been noted that the thickness of the composites slightly increased with an increase of MWCNTs content. Average thicknesses of 3.33, 3.40, 3.54, and 3.75 mm were recorded with MWCNTs contents of 0.0, 0.5, 1.0, and 1.5 wt%, respectively. The maximum increase in thickness was 12.6% with the addition of 1.5 wt% MWCNTs. However, in all cases, fracture occurred only along the midplane of the specimens, so the slight variation in thickness did not affect the fracture toughness of the material. A fiber volume fraction test was performed in accordance with ASTM D3171-06 [33] reporting the weight of fiber reinforcement to be 58%, 50%, 51%, and 49% for MWCNTs contents of 0.0, 0.5, 1.0, and 1.5 wt%, respectively. The increase in the fiber volume fraction associated with increasing the MWCNTs content is expected given the use of same fabrication environment and curing conditions such as applied pressure, temperature and vacuum level for all specimens with different MWCNTs content and would explain the corresponding increase in thickness.

Both thin axial edges of each specimen were coated in white correction fluid, and fine lines were drawn at 1 mm intervals along the length to measure the crack advance. Piano joints were glued to the top and bottom of each specimen at the release film end. The arms of the piano joints were carefully positioned 50 mm before the crack tip and were covered with a thin layer of CFRP gripping in order to prevent slippage or grip failure while testing. A typical DCB specimen is shown schematically in Figure 4.

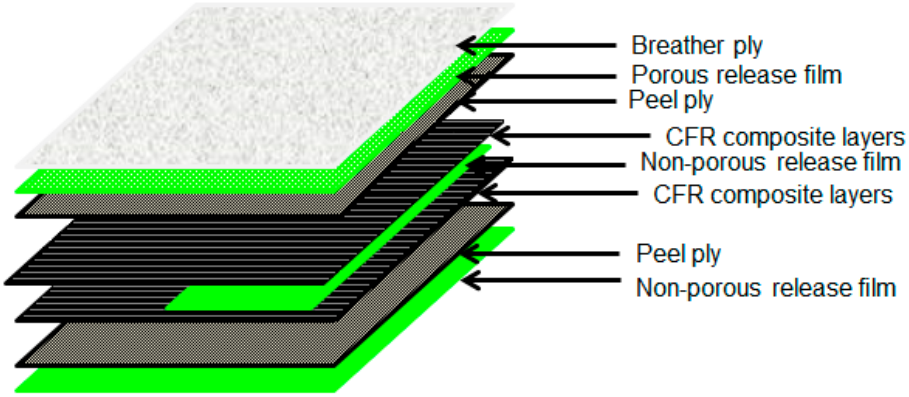

Figure 3. The order of materials used in the hand-layup technique for the fabrication of unidirectional CFRP composite laminates.

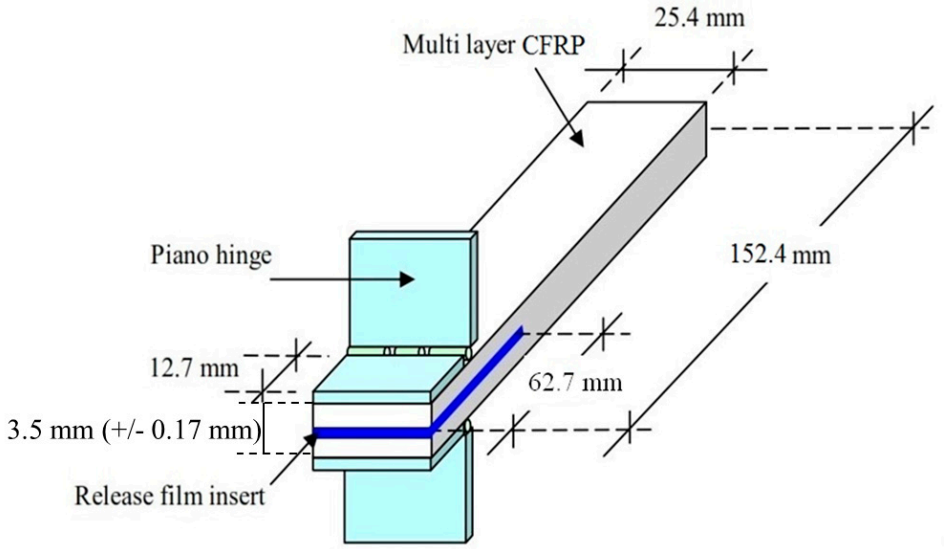

Figure 4. The dimensions of the DCB composite laminate coupons.

2.4. Mode I Fracture Testing Setup

To evaluate mode I interlaminar fracture toughness, DCB tests were performed in accordance with ASTM standards [34]. Five specimens were tested for each of the four MWCNTs contents (0.0, 0.5, 1.0, and 1.5 wt%). The DCB specimens were loaded in tension using an MTS Bionix servo-hydraulic machine. The displacement control was set at a crosshead rate of 0.5 mm/min. An LED illuminated digital optical microscope was used to visually observe and record the crack propagation along the edge of each specimen as shown in Figure 5. For every millimeter of crack propagation, the time was recorded. The load P and the opening displacement δ were recorded by the MTS, Eden Prairie, MN, USA load cell every 10 s. This relatively low frequency sampling rate was sufficient to record the delamination growth every 5 mm as suggested by ASTM standards. This data was then correlated with the occurrence of crack propagation as a function of time. Figure 6 displays a series of recorded steps of the visual crack propagation for a 1.0 wt% MWCNTs specimen alongside the plotted load and opening displacement data.

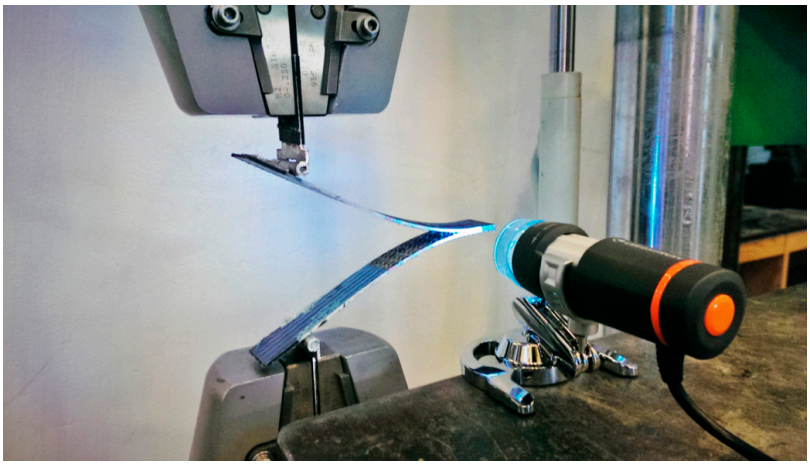

Figure 5. The DCB test setup with an optical microscope used to monitor and record the delamination growth.

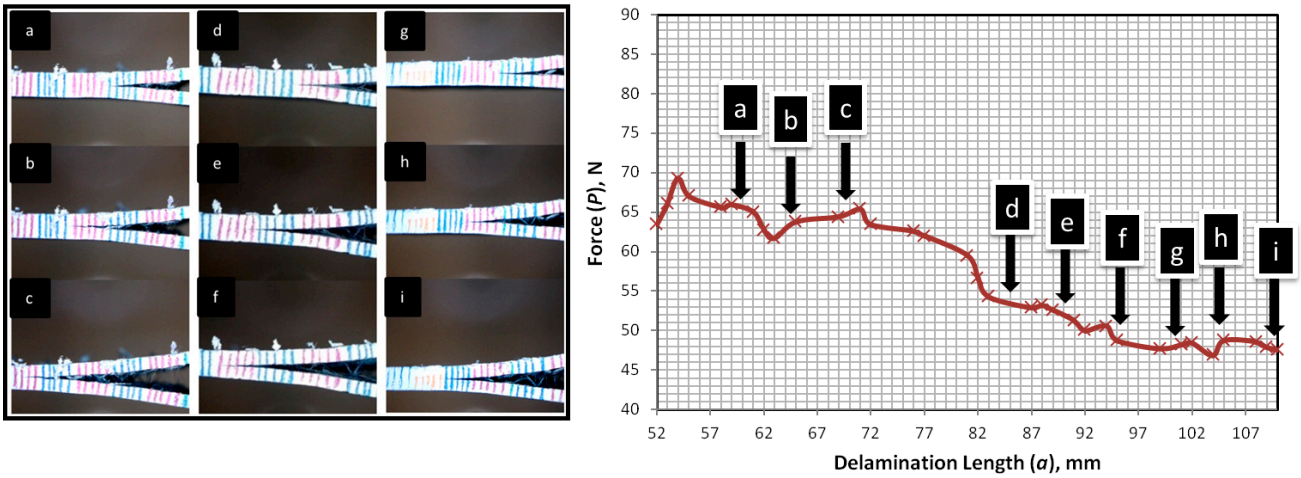

Figure 6. The crack propagation observed in a 1.0 wt% COOH–MWCNTs CFRP composite (**left**) with the associated load-displacement behavior (**right**).

The modified beam theory (MBT) method was applied for data analysis as a conservative estimate of the energy release rate G_{IC} [34]. G_{IC} was used to quantify the mode I interlaminar fracture toughness. The load P and opening displacement δ for each instance of 1 mm crack propagation were used to solve for compliance C using Equation (1):

$$C = \frac{\delta}{P} \tag{1}$$

The delamination length a was corrected as per ASTM standards using the crack length correction Δ. Δ was determined experimentally by generating a least-squares plot of the cubed root of compliance $C^{1/3}$ as a function of the delamination length. This plot was fitted linearly, and Δ was determined by calculating the absolute value of the x-intercept of the fitted line. G_{IC} was then calculated based on the corrected linear elastic fracture mechanics (LEFM) Modified Beam Theory formula using Equation (2):

$$G_{IC} = \frac{3P\delta}{2b(a+\Delta)} \tag{2}$$

where P is the applied load, δ is the opening displacement, b is the specimen width, a is the delamination or crack length, and Δ is the correction for the delamination length. Furthermore, ASTM suggested reducing the energy release rate by correction factor F in Equation (3) in order to account for large deformation and shortening of the moment arm:

$$F = 1 - \frac{3}{10}\left(\frac{\delta}{a}\right)^2 - \frac{3}{2}\left(\frac{\delta t}{a^2}\right) \tag{3}$$

where t is the vertical distance between the load application in the center of piano hinge and half the midplane of the cantilever arm. The initial G_{IC} was calculated at the onset of delamination crack growth. The subsequent energy release rates were calculated for each additional millimeter of crack propagation. LEFM was applied as per ASTM D5528 [34], because the damage zone of delamination was small relative to the smallest specimen dimension.

2.5. Flexural Testing

A three-point bending test was performed in accordance with ASTM D790-10 [35] to determine the bending elastic modulus E_b of the composite laminates as:

$$E_b = \frac{L^3 m}{4bd^3} \tag{4}$$

where L is the span length, m is the slope of the force-displacement curve, b is the specimen width, and d is the specimen depth. The setup for this test is depicted in Figure 7.

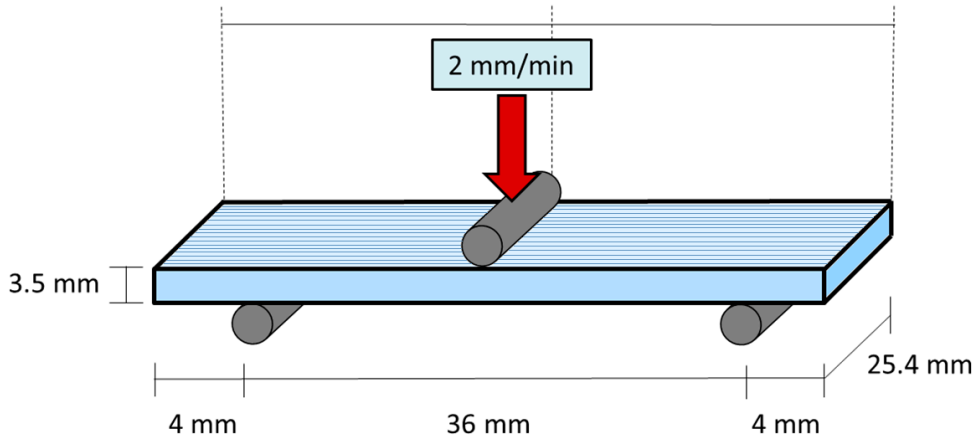

Figure 7. The specimen geometry used for the bending test of unidirectional CFRP.

2.6. Spectroscopic Analysis

Fourier transform infrared (FTIR) spectroscopy was performed using a biconical reflectance Nicolet Nexus, Ramsey, MN, USA, 670 micro-Fourier transform infrared spectrometer (micro-FTIR) (Thermo Fisher Scientific, Waltham, MA, USA) containing a continuum microscope with a Globar source, an XT-KBr beam splitter, and a MCT-A detector with area of 100 × 100 μm^2 and a 4 cm^{-1} resolution. One 25.4 mm × 25.4 mm sample was extracted from the fracture surface of each of the four CFRP specimen types containing different MWCNTs contents. X-ray photoelectron spectroscopy (XPS)

was perform on one 1 mm × 1 mm sample extracted from the fracture surface of each of the four CFRP specimen types containing different MWCNTs contents, as well as the carbon fiber fabric.

2.7. Finite Element Modeling

The DCB specimens were numerically modeled using the finite element (FE) method via ABAQUS 6.13. The purpose of the FE model was to better understand the effect of MWCNTs on CFRP interlaminar fracture toughness parameters. This was achieved by performing back-calculation analysis on our experimental data to extract the fracture parameters for the normal stress-opening displacement relationship for each of the four MWCNTs contents. The experimental data collected for mode I interlaminar fracture toughness was used to model the delamination phenomenon observed in the tested composite laminates. The FE model was developed using the cohesive zone material (CZM) modeling technique. CZM is a nonlinear damage modeling technique used to simulate crack initiation and propagation at the fracture surface during the delamination process [36]. It does so by describing the cohesive forces acting on the crack surface [37]. The main advantage of this technique is that the damage experienced by specimens containing various MWCNTs contents can be predicted and displayed separately, allowing for distinction between different failure scenarios. The CZM technique was used to verify via numerical modeling that failure occurred only along the delamination surface.

The dimensions of the modeled DCBs were equivalent to those tested. Each of the four specimen types was modeled using the specific thickness of the representative specimen for that MWCNTs content. The CFRP composite laminate was defined as a transversely isotropic, linear elastic material. Because of its significant effect on the flexural rigidity of DCB tests, E_1 of the composite laminate was determined experimentally through the flexural tests for each specimen with specific MWCNTs content. The elastic moduli of bending of the composite laminates were calculated for each specimen type, and the results are presented in Table 1 below. Other laminate properties were assumed the same for different types of specimens, and they were determined using the rule of mixture (ROM) and classical lamination theory (CLT) based on fiber and matrix properties. In this case, E_2, G_{12}, ν_{12}, and ν_{23} were calculated as 6.5 GPa, 2.57 GPa, 0.3, and 0.4 respectively.

Table 1. Elastic modulus of the carbon fiber reinforced polymer (CFRP) composite laminate in fiber direction (E_1) obtained experimentally for specimens with different multi-walled carbon nanotubes (MWCNTs) content.

wt% MWCNTs	0.0%	0.5%	1.0%	1.5%
E_1 (GPa)	32.1	30.3	32.9	36.5

To simulate the load application with piano hinges, a vertical displacement of 60 mm was applied to an edge node in the top half of the cantilever at a distance of 12.7 mm from the left edge using an equation constraint to bind the remaining nodes along the transverse axis. A pinned support was defined along the bottom half of the cantilever at the same distance from the edge as the top displacement, allowing for free rotation of the cantilever beam, while preventing shear stresses from occurring at the interface and mode II delamination growth, as was the case experimentally.

A third 3D deformable solid part was created with the interface dimension and a zero thickness to simulate a cohesive surface. This approach was used to define the bond between the two halves of the

cantilever beam and to specify the failure criteria for delamination. The first 62.5 mm of the modeled DCB contained no contact interaction definition to simulate the initial delamination length created in the experiment by the release film insert. The remaining length of the model contained the CZM layer and simulated the region where fracture occurred in the experimental specimens. Tie constraints were used to define the contact between the cohesive layer and the top and bottom halves of the cantilever beam.

Three characteristic parameters were used to define the bilinear stress-crack opening displacement relationship: σ_{bond}, G_{IC}, and K. The values were back-calculated such that the finite element model was able to accurately simulate the load-displacement observation of the DCB test. For all cases, it was assumed that the maximum normal stress σ_{bond} was the interlaminar tensile strength selected to fit the onset of crack propagation. The stiffness K was the ascending slope of the stress-crack opening displacement curve and was selected such that the finite element model simulation matched the ascending branch of the observed load-displacement curves. G_{IC} was taken to be the maximum energy release rate obtained experimentally for each of the MWCNTs contents.

Delamination behavior is governed by the triangular tensile stress-crack opening displacement relationship that can be viewed schematically in Figure 8. This behavior, observed as an increase in normal stress σ, will take place until the maximum interfacial bond strength σ_{bond} is reached. This will be followed by a decrease in stress until fracture takes place when the opening displacement reaches its maximum value of δ_t. The area under the normal stress-crack opening displacement relationship represents the mode I critical energy release rate G_{IC} and can be expressed using Equation (5):

$$G_{IC} = \frac{1}{2}\sigma_{bond}\delta_t \tag{5}$$

This equation was used to solve for δ_t. From geometry, δ_{bond} was solved for using Equation (6).

$$\delta_{bond} = \frac{K}{\sigma_{bond}} \tag{6}$$

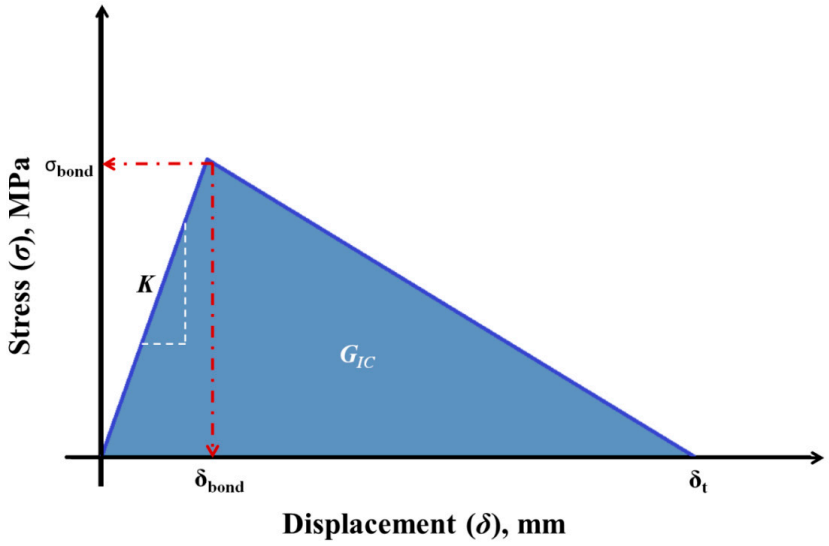

Figure 8. A schematic for the bilinear relationship for CZM elements at the composite laminate interface.

3. Results and Discussion

3.1. Experimental Fracture Tests

Figure 9 depicts a comparison of the load-displacement curves between the four tested MWCNTs contents. The maximum load and stiffness of the 1.5 wt% MWCNTs composite specimen displayed an increase compared to the other three specimen types. The maximum load and stiffness of the 1.0 wt% MWCNTs content specimen remained about the same as the neat specimen, while the 0.5 wt% MWCNTs content specimen dropped slightly in terms of maximum load and stiffness.

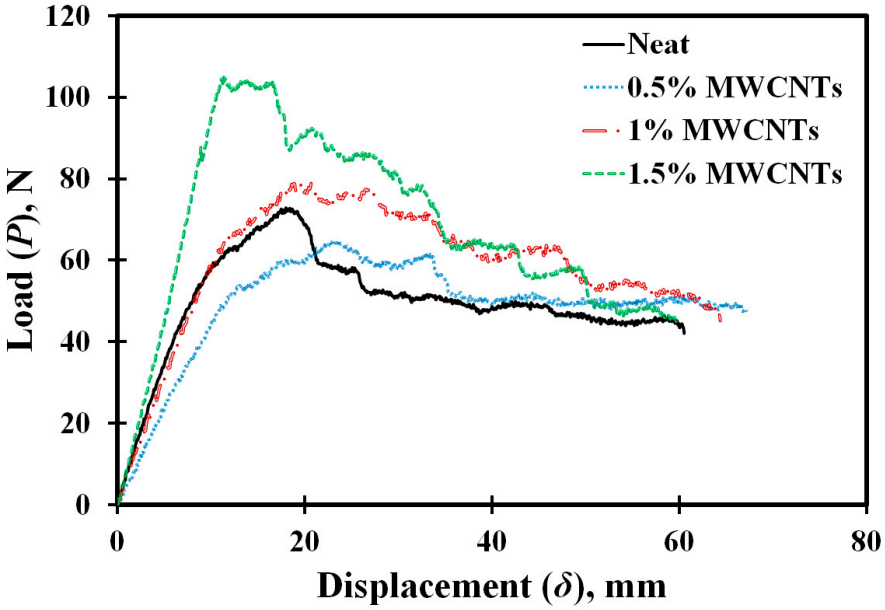

Figure 9. The load-displacement curves for the four representative MWCNTs content specimens.

The resistance curves (*R*-curves) in Figure 10 display the representative median curves of the mode I interlaminar fracture toughness as a function of the delamination length observed for each of the MWCNTs contents. The experimental data points were fitted using power functions to represent the trend of fracture toughness. The experimental results show that the incorporation of MWCNTs increased the interlaminar fracture toughness G_{IC} compared with neat CFRP. Specimens incorporating 0.5 wt% MWCNTs also exhibited the largest maximum increase in fracture toughness compared with other MWCNTs contents examined in this study. The maximum interlaminar fracture toughness G_{IC} for the 0.5 wt% MWCNTs content specimens was 1.17 kJ/m^2. This result is 25% higher than the fracture toughness of the neat CFRP, which had a maximum G_{IC} of 0.94 kJ/m^2. The increase of the maximum G_{IC} for the 1.0 and 1.5 wt% MWCNTs content specimens compared with the neat case is 20% and 17%, respectively. The difference in the maximum G_{IC} for the four specimen types is shown in Figure 11. Statistical analysis using student *t*-test with a 95% level of confidence show that the only experimental group with a statistical significant difference in G_{IC} is that containing a 0.5 wt% MWCNTs content.

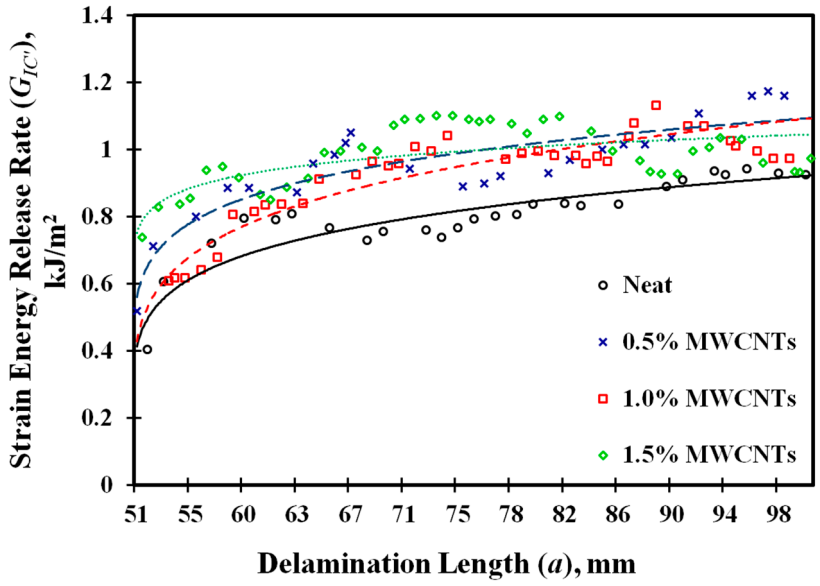

Figure 10. The resistance curves (*R*-curves) for the MWCNT/epoxy unidirectional CFRP composites.

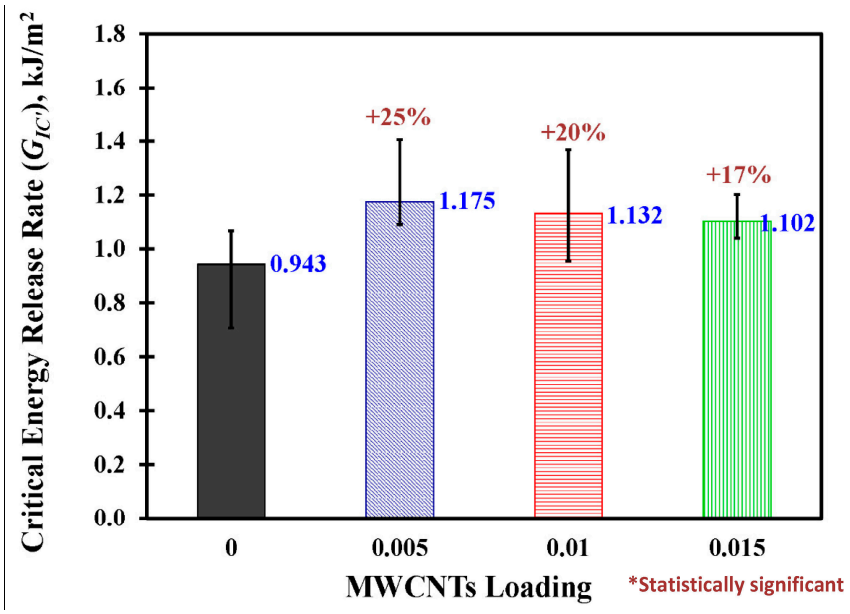

Figure 11. A comparison of the maximum critical energy release rates for the four MWCNTs content specimens. Maximum G_{IC} values are shown on graph. Percentages shown above bars represent the difference (improvement) compared with the neat composite.

It is believed that in neat CFRP laminates, delamination occurs due to tensile cracking of the matrix associated with bridging of carbon fibers, which provides resistance against delamination growth at the crack tip. When MWCNTs are added, a similar mechanism remains; however, an additional energy consumption mechanism is developed where the MWCNTs also bridge the interface of the crack tip and provide increased resistance against crack propagation. An LED illuminated digital optical microscope was used to examine the fracture surface morphology of specimens containing 0.0, 0.5, 1.0, and 1.5 wt% MWCNTs, displayed in Figure 12a–d, respectively. The surface of the neat specimen displays relatively smooth epoxy. The remaining three specimens show evidence of MWCNTs pull-out and fiber bridging observed in their rough fracture surface. Li *et al.* [15] confirmed that composites containing CNTs

produced rougher fracture surfaces compared with composites without CNTs. This is likely due to a toughening effect taking place in the matrix. Toughening can hinder crack propagation by reducing stress concentrations and producing a strong interphase. Davis *et al.* [5] found similar results showing that the surface of the neat specimens displayed a planar fracture path compared with the specimens containing CNTs that had jagged fracture paths. Jagged fracture paths (known as crack branching) rather than smooth fracture paths are evidence of the creation of new means of energy consumption at the fracture process zone and thus improvement of fracture toughness. The increase in fracture toughness with the addition of COOH–MWCNTs may also lead to improvements on the tensile properties of CFRP as reported by Soliman *et al.* [20]. It was found that with the addition of 0.5 wt% COOH–MWCNTs, improvements of 13% and 21% can be obtained in the off-axis tensile strength and ductility, respectively.

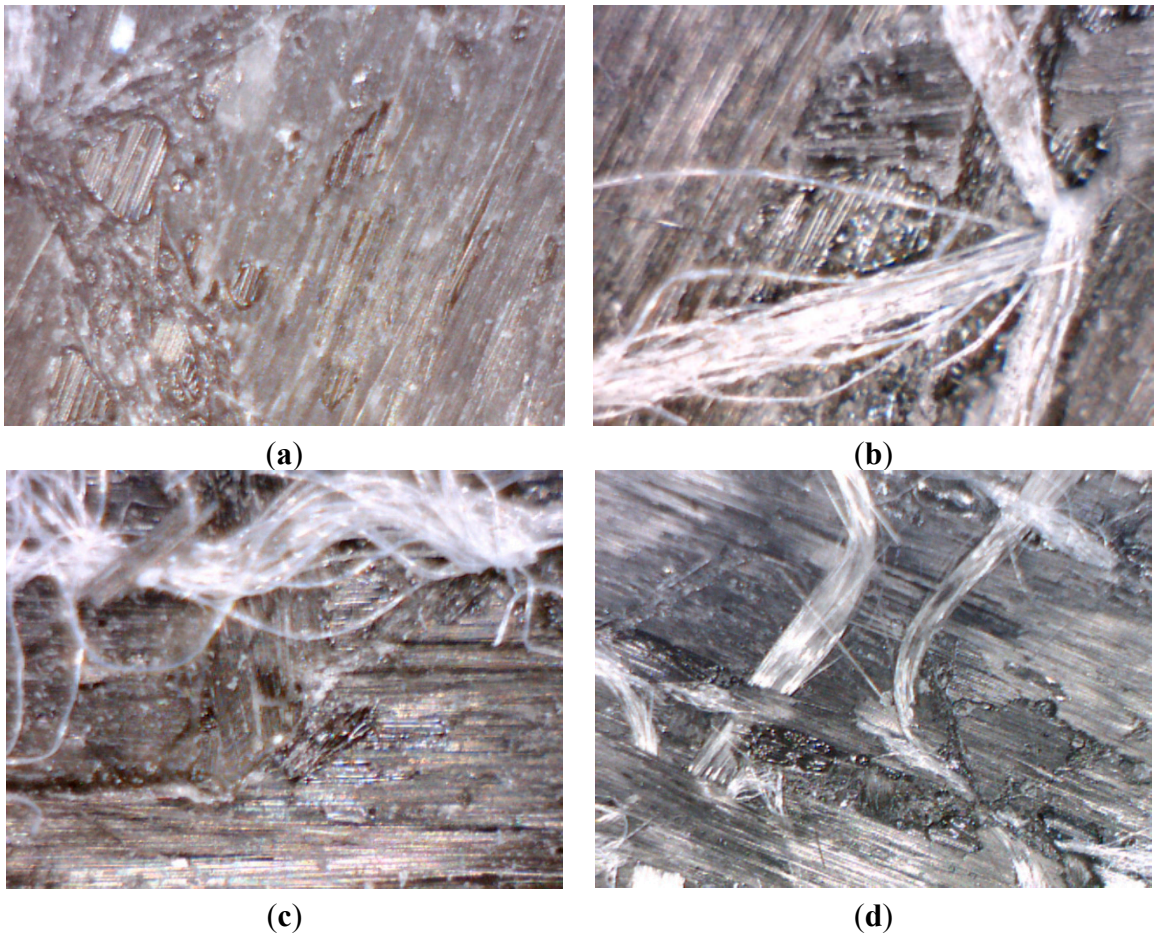

Figure 12. The fracture surface morphology of specimens containing (**a**) 0.0 wt%, (**b**) 0.5 wt%, (**c**) 1.0 wt%, and (**d**) 1.5 wt% MWCNTs.

While this mechanism described above might explain the improvement of interlaminar fracture toughness observed with the addition of 0.5 wt% MWCNTs, it cannot explain the reduced improvement of fracture toughness observed as the MWCNTs content increased further. It was noted during fabrication that as the MWCNTs content increased, the nanocomposite epoxy mixture became more viscous at room temperature compared with the neat epoxy. The increased viscosity was temporarily overcome during the dispersion of MWCNTs by rising the epoxy temperature. This ensured that all MWCNTs were well-dispersed independent of the MWCNTs content. Scanning electron microscope

(SEM) images in Figure 13 verify the good dispersion of different contents of MWCNTs in epoxy matrix. In the figure, the yellow arrows mark some of the embedded MWCNTs. While the dispersion of MWCNTs is fair for the three MWCNTs contents, it is obvious from the SEM images that the intensity of MWCNTs increase as the MWCNTs content increases. Nevertheless, the fabrication of the composite specimens was not performed until the epoxy had been cooled to room temperature. Therefore, it follows that the increased viscosity of the epoxy-MWCNTs nanocomposite had some effect on the fabrication of CFRP laminates, which is dependent on the ability of the epoxy to impregnate the carbon fiber fabric plies. This observation illuminates the fact that when using MWCNTs, one must consider two competing factors: first, the ability of MWCNTs to improve the composite material characteristics, and second, the significance of the effect of MWCNTs on epoxy viscosity, which can hinder the fabrication of CFRP laminates and their resultant material characteristics. Another factor that may influence the interlaminar fracture toughness is the effect of MWCNTs on the curing of resin. Relatively large amounts of COOH–MWCNTs may affect the chemical reaction between the epoxy group in the resin and the amine group in the hardener, which in turn may affect the cross-linking process. In addition, the MWCNTs may affect the bond between the resin and the sizing coating in fibers which would also influence the interfacial bond between the fibers and the resin. More investigations are required to understand the chemical effect of adding MWCNTs.

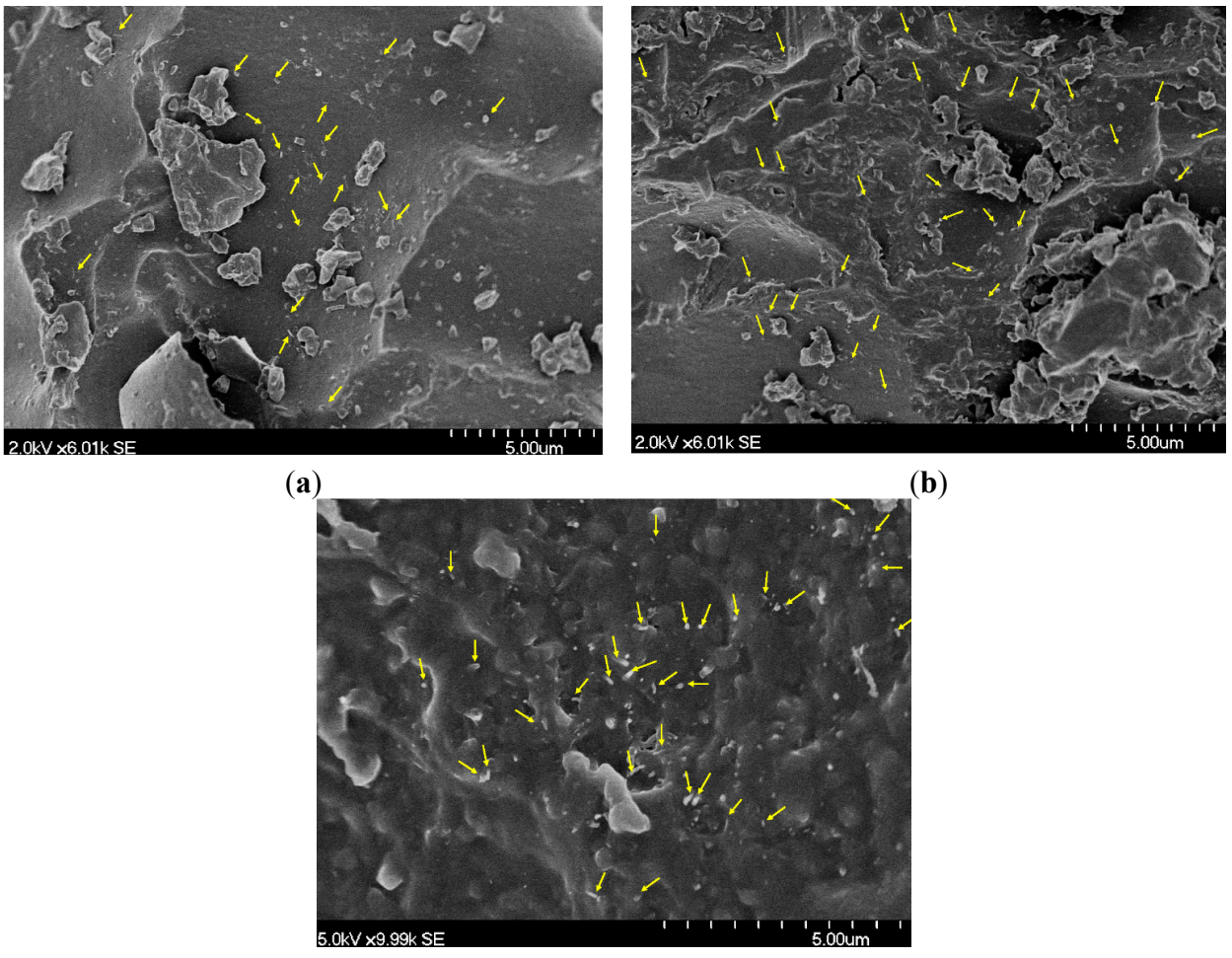

Figure 13. SEM images for specimens containing (**a**) 0.5 wt%, (**b**) 1.0 wt%, and (**c**) 1.5 wt% MWCNTs showing the dispersion of MWCNTs in the epoxy matrix.

3.2. Fourier Transform Infrared Measurements

To further explain the effects of MWCNTs on epoxy, Fourier transform infrared (FTIR) measurements were collected to determine if a chemical reaction between the functionalized MWCNTs and epoxy at the fracture surface had taken place. For comparison four specimen samples were analyzed, one of each of the MWCNTs contents. When analyzing the FTIR spectroscopy, a comparison should be made between peak locations along each wavelength. A shift in the vibration peak location would indicate that a chemical reaction had taken place. The units of the y-axis are arbitrary and are to be used only for the purpose of identifying the realization of spectrogram peaks. The vibration peaks of the four different epoxy nanocomposites with varying MWCNTs contents can be observed in Figure 14.

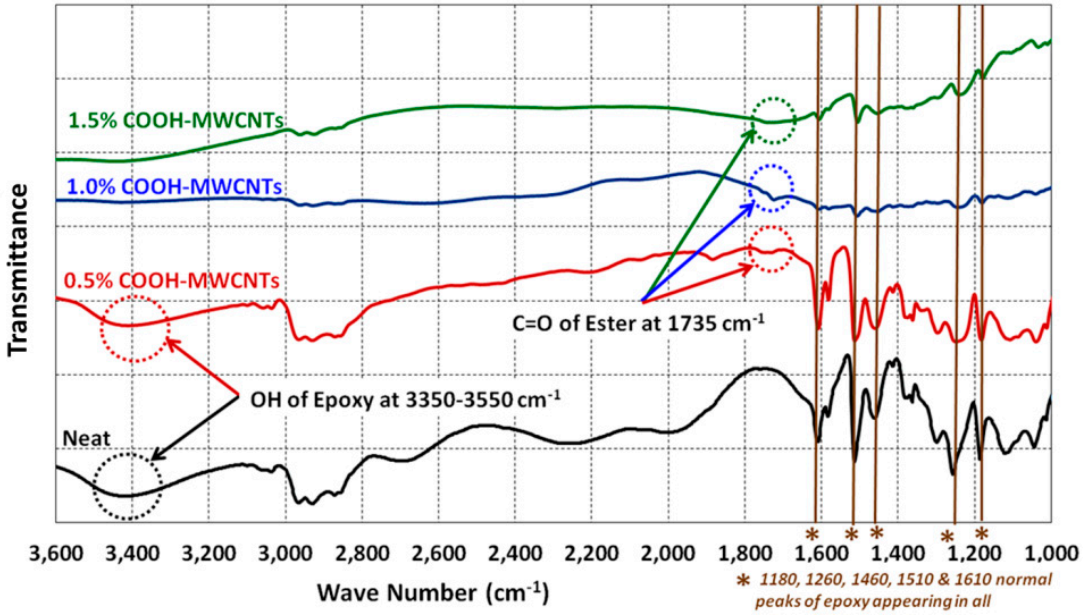

Figure 14. The peaks observed in the FTIR spectroscopy for samples of the four MWCNTs contents.

The FTIR analysis shows that all epoxies with and without MWCNTs display the standard epoxy peaks observed at 1180, 1260, 1460, 1510, and 1610 cm^{-1}. Epoxy incorporating 0.5 wt% and 1.0 wt% MWCNTs show the C=O stretch at 1735 cm^{-1}, indicating that an esterification reaction between the epoxy resin and the COOH group of the surface functionalized MWCNTs took place during fabrication. This shift at 1735 cm^{-1} has been reported by Zou *et al.* [38] and Kim *et al.* [27] as the result of direct coupling between the carboxylic groups in the MWCNTs and the hydroxyl groups in the epoxy resin. It is known that epoxy has two sources of hydroxyl group also known as alcoholic part of epoxy. The first hydroxyl group is located in the main epoxy resin before curing. The second hydroxyl group source results from the curing reaction of epoxy resin with hardener [39]. The latter is the one of interest to us in the FTIR analysis. Kim *et al.* [27] reported the potential for such a reaction, explained by the fact that ester is formed when the stoichiometric ratio shifts, allowing one of the reactants to exist in larger excess. Here the amount of epoxy resin is far greater than the amount of COOH. Consequently, this is a strong indicator that the alcoholic part (the epoxy in our case) is in a very large excess which enhances the reversible esterification reaction in the forward direction according to Le Chatelier's principle [40]. In addition, the COOH–MWCNTs were added first to the epoxy resin, and the mixture

was sonicated for 1.0 h at 40 °C. To ensure a chemical reaction between the functional groups on the surface of the nanotubes and the resin chains, the dispersed mixture was stirred for 2.0 h at 80 °C. Direct removal of the produced esterification water by evaporation further favors the forward esterification reaction.

In the neat and 0.5 wt% specimens, a slight drop in transmittance can be observed within the range of 3350–3550 cm^{-1}. The 1.0 wt% and 1.5 wt% MWCNTs specimens contained higher contents of COOH, which is able to react with OH. Therefore, less OH remained available in these specimens. The FTIR results confirm that a reaction between the epoxy and the COOH-functionalized MWCNTs took place to produce a new epoxy-MWCNTs nanocomposite with improved fracture toughness as observed experimentally.

3.3. X-ray Photoelectron Spectroscopy

While FTIR observations provide important evidence of the different reactivity of MWCNTs with the epoxy resin and hardener and the role of the increased content on this reactivity, FTIR observations do not provide quantitative evidence of this reactivity and its implication on the binding energy between the composite and the polymer nanocomposite matrix. To confirm the above observations, XPS analysis was conducted. Analysis of XPS observations shows results for binding energies around 284 eV. The deconvolution of C1 peaks for the COOH–MWCNTs are shown in Figure 15 and presented in Table 2. Five peaks were found, representing C–C groups, C–O/C–N groups, C–O–C epoxy groups, C=O groups, and COOH groups. Similar results were reported by Fang *et al.* [26], Ma *et al.* [41], and Dai *et al.* [42]. The intensity of the C–O–C epoxy group identified at a binding energy of 287.1 eV decreases as the MWCNTs content increases. The epoxy group reacts with the amine group in the hardener and the carboxyl group in the MWCNTs. Since the resin to hardener ratio is constant among all specimens, this decrease can only be attributed to the reaction between C–O–C of the epoxy group and COOH, which relates to the increase of COOH–MWCNTs content. This provides quantitative evidence of a chemical reaction between the MWCNTs and epoxy. At the binding energy of 289.2 eV, the COOH groups increase with the increase of MWCNTs content, which indicates the content of MWCNTs in each specimen. XPS observations are thus in good agreement with FTIR observations.

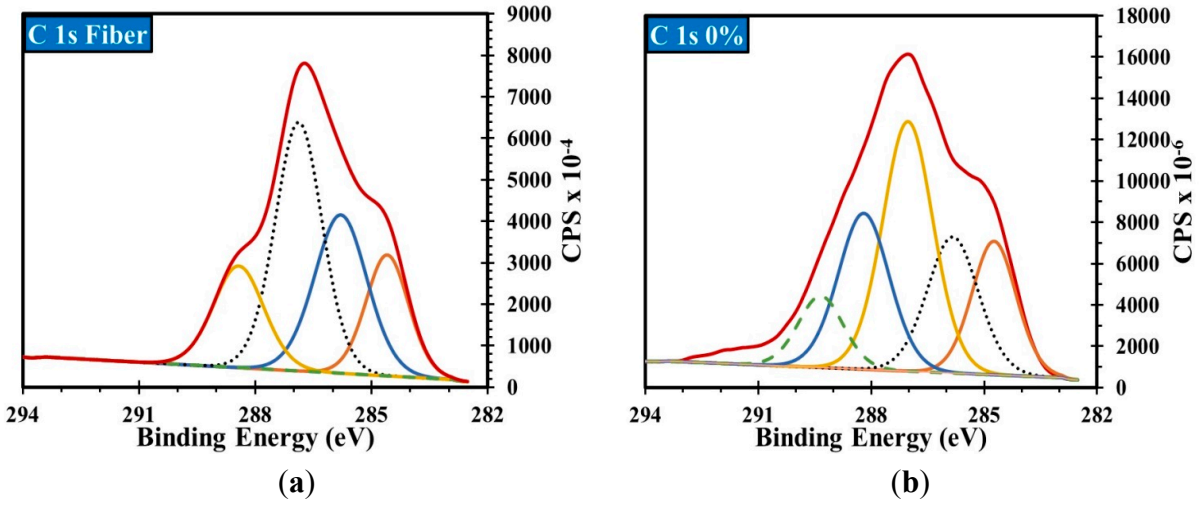

Figure 15. *Cont.*

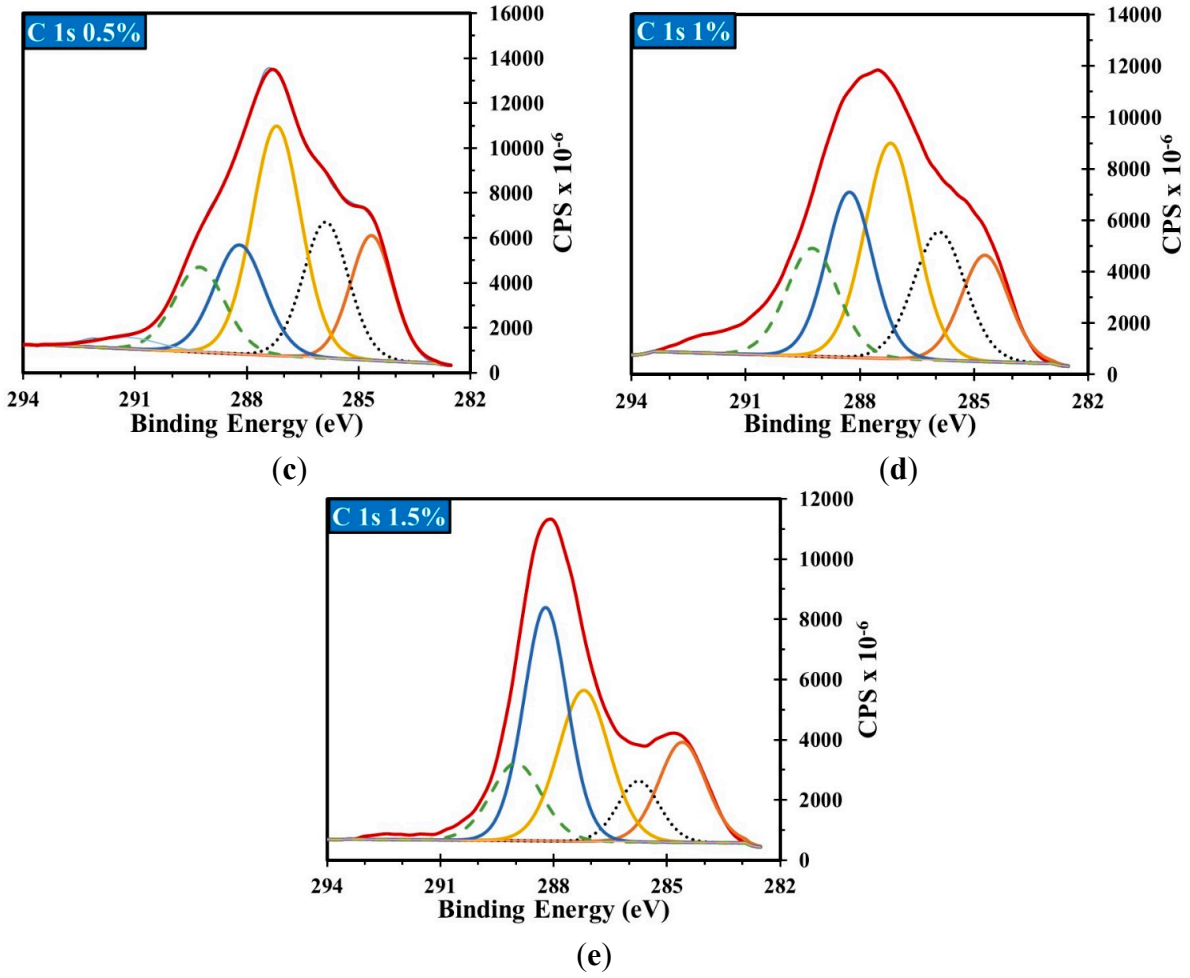

Figure 15. XPS analysis showing the deconvolution of binding energies of carbon C1 peaks for (**a**) a carbon fiber fabric sample, (**b**) a 0.0 wt%, (**c**) 0.5 wt%, (**d**) 1.0 wt%, and (**e**) 1.5 wt% MWCNTs sample.

Table 2. C1s peak fitting results for specimens with different MWCNTs contents.

Chemical bond/group		C–C%	C–O% & C–N%	C–O–C% Epoxy group	C=O%	COOH%
Binding energy (eV)		284.6	285.8	287.1	288.3	289.2
Specimen	Fibers	14.3	22.7	44.5	18.5	-
	Neat Epoxy	18.1	21.0	33.7	16.3	8.7
	0.5% COOH–MWCNTs	14.9	21.2	33.4	15.4	12.5
	1.0% COOH–MWCNTs	13.6	18.0	32.7	19.7	15.7
	1.5% COOH–MWCNTs	13.5	7.3	20.4	39.2	16.8

The occurrence of pure interlaminar fracture failure at the midplane only was verified using a bending test. The bending test results, displayed in Figure 16, show that the bending strength of the CFRP specimens was 364.4 and 262.7 MPa for the neat and 0.5 wt% MWCNTs contents, respectively. Given that the maximum moment experienced by the neat and 0.5 wt% MWCNTs specimens was 4493 and 3711 N·mm, respectively, the bending stress developed in the DCB test was only 7%–8% of the flexural strength. At this stress level, the load-displacement response is linear elastic, and no nonlinearity due to

delamination was observed which confirms that the fracture was a result of interlaminar delamination at the midplane of CFRP and did not occur in the cantilever arms.

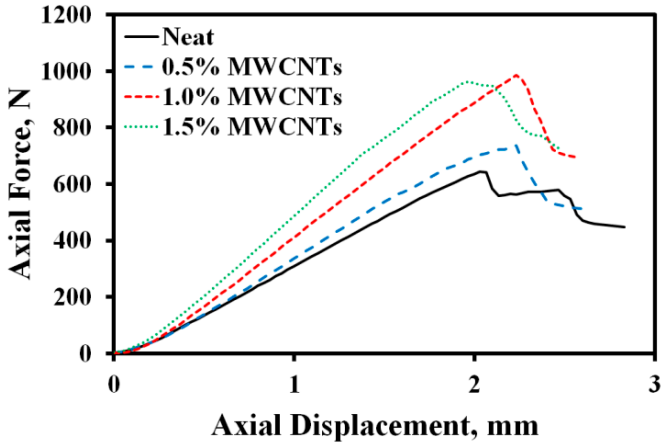

Figure 16. A depiction of the flexural test results.

3.4. Finite Element Validation

FE simulations were performed for the two significant specimens of interest based on the experimental results: neat and 0.5 wt% MWCNTs. A deformed FE model representing the neat DCB specimen is depicted in Figure 17. Examining the numerical model, the load-displacement responses for the FE simulation are in good agreement with the experimental results for the neat and 0.5 wt% MWCNTs contents as shown in Figure 18a and b, respectively. However, it is noted that in using LEFM to describe the FE model, a constant critical energy release rate G_{IC} (defined here as the maximum G_{IC} for each representative MWCNTs content specimen) was used. This is inconsistent with the experimental observations, which show that the energy release rates vary with delamination growth. Classical fracture criteria do not take into account the extra fracture mechanisms at work in nanocomposites. For example, other studies showed that viscoelasticity and plasticity for nonlinear matrix material, fiber bridging, and the large deformations of the cantilever arms would introduce nonlinearity in the load-displacement response that is not considered in LEFM [43–45]. In addition, modified beam theory (MBT) assumes that $C^{1/3}$ is a linear function of crack length, but this is only true in the case when fracture toughness has a constant value during crack propagation. In the case of large scale bridging, the experimental points form a curved line, and therefore linear fitting procedures cannot be used to find the correction [6,18]. Nonlinear fracture mechanics would be a better approach to evaluate fracture parameters in DCB [44]. Ideally, using elastic-plastic fracture mechanics, the values of G_{IC} in the FE simulation should vary along the length of delamination, following the trend observed in the experimental *R*-curves. The discrepancy between the experimental and numerical results is thus attributed to the LEFM assumptions used in the FE model which do not necessarily match the crack growth observations. The addition of MWCNTs obviously enlarged the nonlinearity of the interlaminar fracture toughness of CFRP. The use of other fracture mechanics approaches, such as elastic-plastic fracture mechanics or quasi-brittle fracture mechanics, and other fracture toughness parameters, such as J_{IC} in lieu of G_{IC}, might enable better simulation of the observed interlaminar fracture in CFRP laminates incorporating MWCNTs. Nevertheless, the FE model provides insight to explain the observed effect of MWCNTs on interlaminar

fracture of CFRP. LEFM is utilized to calculate fracture toughness in this investigation following ASTM D5528 standards and others [3,6,13,14,34] to compare between different specimens and study the effect of COOH–MWCNTs on the delamination growth.

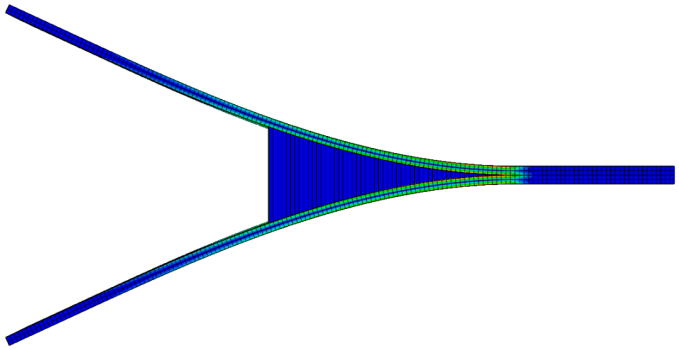

Figure 17. The finite element (FE) simulation of a DCB test using CFRP composite laminates.

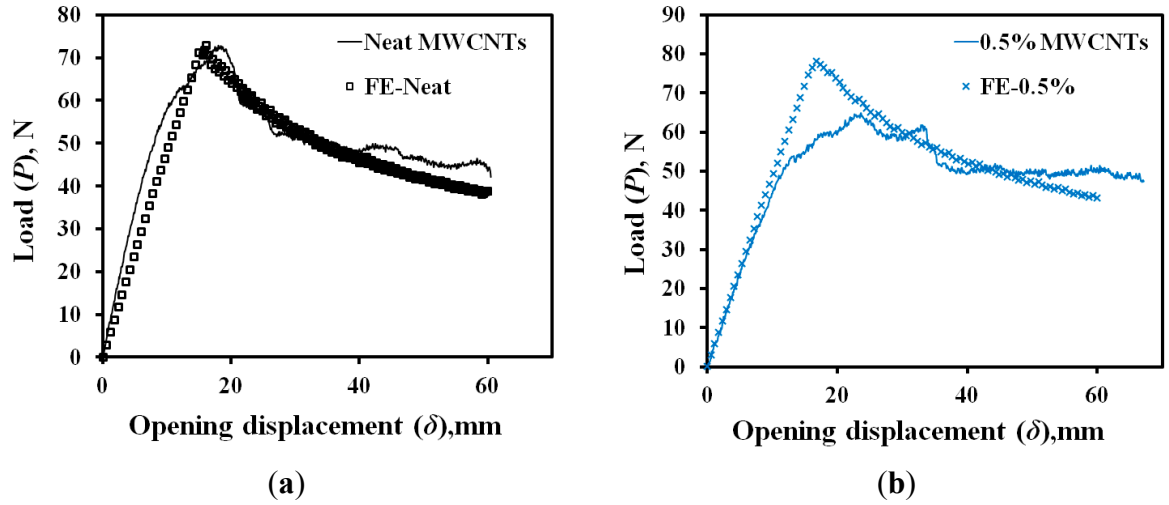

Figure 18. Comparison between the experimental and numerical load-displacement responses for unidirectional CFRP composites containing (**a**) neat and (**b**) 0.5 wt% MWCNTs.

Comparisons between the experimental and numerical results for the delamination growth *vs.* load (Figure 19a,b) and delamination growth *vs.* displacement (Figure 19c,d) for the neat and 0.5 wt% MWCNTs specimens have been made. These comparisons confirm that the FE model is capable of predicting the delamination growth observed experimentally. The cohesive crack model parameters were optimized to enable the FE model to match the experimental observation of the delamination growth *vs.* load and crack opening displacement. The normal stress-crack opening displacement behavior for the neat and 0.5 wt% MWCNTs specimens describing the cohesive crack model is shown in Figure 20. The optimal cohesive crack model parameters infer that a 22.5% increase in opening displacement for the 0.5 wt% MWCNTs specimen compared with the neat specimen is necessary to simulate the experimental observations. The extracted cohesive model parameters, as shown in Figure 20, confirm that MWCNTs improve the interlaminar fracture toughness of unidirectional CFRP.

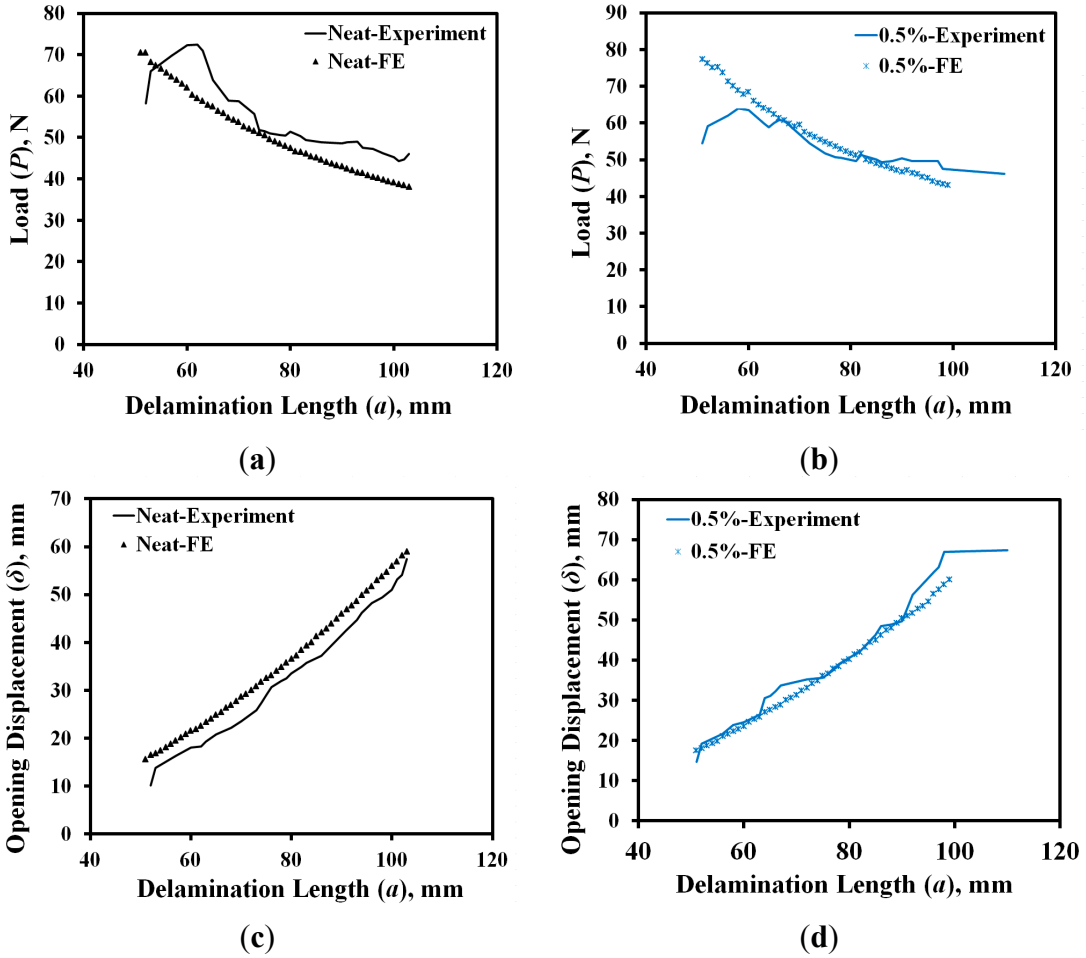

Figure 19. Comparison between the experimental and numerical behavior of (**a**) delamination growth *vs.* load for unidirectional CFRP composites with 0.0 wt% MWCNTs and (**b**) 0.5 wt% MWCNTs, (**c**) delamination growth *vs.* opening displacement for unidirectional CFRP composites with 0.0 wt% MWCNTs and (**d**) 0.5 wt% MWCNTs.

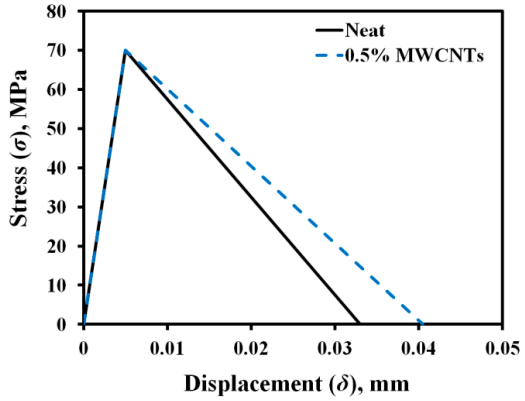

Figure 20. The normal stress-crack opening displacement relationships for unidirectional CFRP composites containing neat and 0.5 wt% MWCNTs.

4. Conclusions

CFRP DCB specimens were experimentally tested and numerically modeled to examine the effect of incorporating MWCNTs on the mode I interlaminar fracture toughness of composite laminates.

Three contents of COOH–MWCNTs (0.5 wt%, 1.0 wt%, and 1.5 wt%) were examined and compared with neat epoxy specimens. Values of fracture toughness G_{IC} were determined and compared among the four specimen types. The experimental results show a 25% statistically significant increase in the interlaminar fracture toughness G_{IC} of the 0.5 wt% MWCNTs content specimens compared with neat CFRP specimens. However, limited increases of 20% and 17% in G_{IC} were observed for specimens incorporating 1.0 wt% and 1.5 wt% MWCNTs contents respectively, compared with neat CFRP specimens. Microstructural investigations using FTIR and XPS confirmed the occurrence of chemical reaction between the COOH–MWCNTs and epoxy resulting in the formation of a new epoxy-MWCNTs nanocomposite with improved interlaminar fracture toughness. In addition, microscopic images using an LED illuminated digital optical microscope confirmed that the new type of epoxy-MWCNTs nanocomposite enabled additional energy consumption mechanisms (e.g., crack branching) compared with those observed in the neat epoxy specimens. CFRP fabricated with epoxy-MWCNTs nanocomposites exhibit a higher value of interlaminar fracture toughness than CFRP fabricated with neat epoxy.

An increase in MWCNTs content did not result in further improvement of the interlaminar fracture toughness of CFRP. This observation has been attributed to the adverse effect that a high content of MWCNTs had on epoxy viscosity during fabrication, which hindered its ability to flow and impregnate the carbon fiber cloth, thus producing CFRP composites with insignificantly improved interlaminar fracture toughness.

A finite element model was developed to simulate the delamination growth process and to further infer the effect of MWCNTs on the fracture behavior at the composite interface. The validated FE model showed a 22.5% increase in maximum crack opening displacement for CFRP with 0.5 wt% MWCNTs compared with CFRP containing neat epoxy. The above research suggests that as a structural material, CFRP composite laminates produced with a low content of COOH–MWCNTs (~0.5 wt%) would provide advantages in aerospace and infrastructural applications that require improved interlaminar fracture toughness and high crack propagation resistance.

Acknowledgements

This research was partially funded by the Air Force Office of Scientific Research (AFOSR), Award # FA9550-14-1-0021 to the University of New Mexico, and the New Mexico Space Grant Fellowship to the first author. The authors acknowledge both supports. The third author greatly acknowledges funding by the Science and Technology Development Fund (STDF) for Award No. 3713, and the (STDF-CSE) Program (ID 5213) to Polymer Nanocomposites Center, Egyptian Petroleum Research Institute (EPRI), Cairo, Egypt. All the authors would also like to thank Sherif Aboubakr for his initial help in conducting the experiments, Whitney McCutcheon for her assistance in conducting the FTIR spectroscopy and Kateryna Aryushkova for her assistance in conducting the XPS.

Author Contributions

Elisa Borowski and Eslam Soliman fabricated and tested all specimens. Elisa Borowski, Eslam Soliman, and Mahmoud Reda Taha participated in developing the finite element model and analysis of model results. Elisa Borowski, Mahmoud Reda Taha, and Usama Kandil participated in

analysis of microstructural data with FTIR and XPS. The four authors participated in writing the manuscripts. Mahmoud Reda Taha led the team efforts.

Conflicts of Interest

The authors declare no conflict of interest.

References

1. Tsai, J.L.; Huang, H.B.; Cheng, Y.L. Enhancing fracture toughness of glass/epoxy composites for wind blades using silica nanoparticles and rubber particles. *Procedia Eng.* **2011**, *14*, 1982–1987.
2. Tseng, C.H.; Wang, C.C.; Chen, C.Y. Functionalizing carbon nanotubes by plasma modification for the preparation of covalent-integrated epoxy composites. *Chem. Mater.* **2007**, *19*, 308–315.
3. Seyhan, A.T.; Tanoglu, M.; Schulte, K. Mode I and mode II fracture toughness of E-glass non-crimp fabric/carbon nanotube (CNT) modified polymer based composites. *Eng. Fract. Mech.* **2008**, *75*, 5151–5162.
4. Tehrani, M.; Yari Boroujeni, A.; Luhrs, C.; Phillips, J.; Al-Haik, M. Hybrid composites based on carbon fiber/carbon nanofilament reinforcement. *Materials* **2014**, *7*, 4182–4195.
5. Davis, D.C.; Whelan, B.D. An experimental study of interlaminar shear fracture toughness of a nanotube reinforced composite. *Compos. B Eng.* **2011**, *42*, 105–116.
6. Tamuzs, V.; Tarasovs, S.; Vilks, U. Delamination properties of translaminar-reinforced composites. *Compos. Sci. Technol.* **2003**, *63*, 1423–1431.
7. Lubineau, G.; Rahaman, A. A review of strategies for improving the degradation properties of laminated continuous-fiber/epoxy composites with carbon-based nanoreinforcements. *Carbon* **2012**, *50*, 2377–2395.
8. Shu, D.; Mai, Y.W. Effect of stitching on interlaminar delamination extension in composites laminates. *Compos. Sci. Technol.* **1993**, *49*, 165–171.
9. Chen, L.; Ifju, P.G.; Sankar, B.V. A novel double cantilever beam test for stitched composite laminates. *J. Compos. Mater.* **2001**, *35*, 1137–1149.
10. Liu, H.Y.; Mai, Y.W. Delamination fracture mechanics of composite laminates with through-thickness pinning. *Strength Fract. Complex* **2003**, *1*, 139–146.
11. Lenzi, F.; Riccio, A.; Clarke, A.; Creemers, R. Coupon tests on *z*-pinned and unpinned composite samples for damage resistant applications. *Macromol. Sympos. Times Polym. Compos.* **2007**, *27*, 230–237.
12. Woo, E.M.; Bravenec, L.D.; Sefefus, J.C. Morphology and properties of an epoxy alloy system containing thermoplastics and a reactive rubber. *Polym. Eng. Sci.* **1993**, *34*, 1664–1673.
13. Arai, M.; Noro, Y.; Sugimoto, K.I.; Endo, M. Mode I and mode II interlaminar fracture toughness of CFRP laminates toughened by carbon nanofiber interlayer. *Compos. Sci. Technol.* **2008**, *68*, 516–525.
14. Hojo, M.; Ando, T.; Tanaka, M.; Adachi, T.; Ochiai, S.; Endo, Y. Modes I and II interlaminar fracture toughness and fatigue delamination of CF/epoxy laminates with self-same epoxy interleaf. *Int. J. Fatigue* **2006**, *28*, 1154–1165.

15. Li, M.; Gu, Y.; Liu, Y.; Li, Y.; Zhang, Z. Interfacial improvement of carbon fiber/epoxy composites using a simple process for depositing commercially functionalized carbon nanotubes on the fibers. *Carbon* **2013**, *52*, 109–121.
16. Sharma, K.; Shukla, M. Three-phase carbon fiber amine functionalized carbon nanotubes epoxy composite: Processing, characterization, and multiscale modeling. *J. Nanomater.* **2014**, *2014*, 1–10.
17. Park, J.M.; Kim, D.S.; Lee, J.R.; Kim, T.W. Nondestructive damage sensitivity and reinforcing effect of carbon nanotube/epoxy composites using electro-micromechanical technique. *Mater. Sci. Eng. C* **2003**, *23*, 971–975.
18. Ayatollahi, M.R.; Shadlou, S.; Shokrieh, M.M. Mixed mode brittle fracture in epoxy/multi-walled carbon nanotube nanocomposites. *Eng. Fract. Mech.* **2011**, *78*, 2620–2632.
19. Inam, F.; Wong, D.W.; Kuwata, M.; Peijs, T. Multiscale hybrid micro-nanocomposites based on carbon nanotubes and carbon fibers. *J. Nanomater.* **2010**, *2010*, 1–12.
20. Soliman, E.; Al-Haik, M.; Taha, M.R. On and off-axis tension behavior of fiber reinforced polymer (FRP) composites incorporating multiwalled carbon nanotubes. *J. Compos. Mater.* **2012**, *46*, 1661–1675.
21. Patra, A.; Mitra, N. Interface fracture of sandwich composites: Influence of MWCNT sonicated epoxy resin. *Compos. Sci. Technol.* **2014**, *101*, 94–101.
22. Cui, L.; Wang, Y.; Xiu, W.; Wang, W.; Xu, L.; Xu, X.; Meng, Y.; Li, L.; Gao, J.; Chen, L.; *et al.* Effect of functionalization of multi-walled carbon nanotube on the curing behavior and mechanical property of multi-walled carbon nanotube/epoxy composites. *Mater. Des.* **2013**, *49*, 279–284.
23. Zhu, J.; Kim, J.; Peng, H.Q.; Margrave, J.L.; Khabashesku, V.N.; Barrera, E.V. Improving the dispersion and integration of single-walled carbon nanotubes in epoxy composites through functionalization. *Nano Lett.* **2003**, *3*, 1107–1113.
24. Tang, L.C.; Zhang, H.; Han, J.H.; Wu, X.P.; Zhang, Z. Fracture mechanisms of epoxy filled with ozone functionalized multi-wall carbon nanotubes. *Compos. Sci. Technol.* **2011**, *72*, 7–13.
25. Esposito, L.H.; Ramos, J.A.; Kortaberria, G. Dispersion of carbon nanotubes in nanostructured epoxy systems for coating application. *Prog. Org. Coat.* **2014**, *77*, 1452–1458.
26. Fang, C.; Wang, J.; Zhang, T. Interlaminar improvement of carbon fiber/epoxy composites via depositing mixture of carbon nanotubes and sizing agent. *Appl. Surf. Sci.* **2014**, *321*, 1–9.
27. Kim, W.; Kang, S.; Ah, C.; Lee, Y.; Ha, D.; Choi, I.; Yun, W. Functionalization of shortened SWCNTs using esterification. *Bull. Korean Chem. Soc.* **2004**, *25*, 1301–1302.
28. Mujika, F.; Vargas, G.; Ibarretxe, J.; de Garcia, J.; Arrese, A. Influence of the modification with MWCNT on the interlaminar fracture properties of long carbon fiber composites. *Compos. B* **2012**, *43*, 1336–1340.
29. Romhany, G.; Szebenyi, G. Interlaminar crack propagation in MWCNT/fiber reinforced hybrid composites. *Express Polym. Lett.* **2009**, *3*, 145–151.
30. Almuhammadi, K.; Alfano, M.; Yang, Y.; Lubineau, G. Analysis of interlaminar fracture toughness and damage mechanisms in composite laminates reinforced with sprayed multi-walled carbon nanotubes. *Mater. Des.* **2014**, *53*, 921–927.
31. Soliman, E.; Sheyka, M.; Taha, M.R. Low-velocity impact of thin woven carbon fabric composites incorporating multi-walled carbon nanotubes. *Int. J. Impact Eng.* **2012**, *47*, 39–47.

32. *Standard Guide for Preparation of Flat Composite Panels with Processing Guidelines for Specimen Preparation*; ASTM D5687/D5687M–95; ASTM International: West Conshohocken, PA, USA, 2007.
33. *Standard Test Methods for Constituent Content of Composite Materials*; ASTM D3171–06; ASTM International: West Conshohocken, PA, USA, 2006.
34. *Standard Test Method for Mode I Interlaminar Fracture Toughness of Unidirectional Fiber-Reinforced Polymer Matrix Composites*; ASTM D5528–13; ASTM International: West Conshohocken, PA, USA, 2013.
35. *Standard Test Methods for Flexural Properties of Unreinforced and Reinforced Plastics and Electrical Insulating Materials*; ASTM D790–10; ASTM International: West Conshohocken, PA, USA, 2010.
36. Hsu, A.; Mcpheeters, B. *Nastran Cohesive Zone Modeling of Composite Bonded Joints*; Society for the Advancement of Material and Process Engineering (SAMPE): Covina, CA, USA, 2012.
37. Barenblatt, G.I. The mathematical theory of equilibrium cracks in brittle fracture. *Adv. Appl. Mech*. **1962**, *7*, 55–129.
38. Zou, W.; Du, Z.; Liu, Y.; Yang, X.; Li, H.; Zhang, C. Functionalization of MWNTs using polyacryloyl chloride and the properties of CNT-epoxy matrix nanocomposites. *Compos. Sci. Technol*. **2008**, *68*, 3259–3264.
39. Yang, J., III. Part I: Synthesis of Aromatic Polyketones via Soluble Precursors Derived from Bis(A-Amininitrile)S Part II: Modifications of Epoxy Resins with Functional Hyperbranched Poly(Arylene Ester)S. Ph.D. Thesis, Virginia Institute and State University: Blacksburg, VA, USA, 1998.
40. Soliman, E.; Kandil, U.; Taha, M. Improved strength and toughness of carbon woven fabric composites with functionalized MWCNTs. *Materials* **2014**, *7*, 4640–4657.
41. Ma, P.; Mo, S.; Tang, B.; Kim, J. Dispersion, interfacial interaction and re-agglomeration of functionalized carbon nanotubes in epoxy composites. *Carbon* **2010**, *48*, 1824–1834.
42. Dai, Z.; Zhang, B.; Shi, F.; Li, M.; Zhang, Z.; Gu, Y. Effect of heat treatment on carbon fiber surface properties and fibers/epoxy interfacial adhesion. *Appl. Surf. Sci.* **2011**, *257*, 8457–8461.
43. Zhao, W. Mode I Delamination Fracture Characterization of Polymeric Composites under Elevated Temperature. PhD Thesis, Syracuse University, Syracuse, NY, USA, 2011.
44. Biel, A.; Stigh, U. An analysis of the evaluation of the fracture energy using the DCB-specimen. *Arch. Mech.* **2007**, *59*, 311–327.
45. Blackman, B.R.K.; Hadavinia, H.; Kinloch, A.J.; Paraschi, M.; Williams, J.G. The calculation of adhesive fracture energies in mode I: revisiting the tapered double cantilever beam (TDCB) test. *Eng. Fract. Mech.* **2003**, *70*, 233–248.